

Revisiting the DeepWater Horizon spill: High resolution model simulations of effects of oil droplet size distribution and river fronts

Lars R Hole¹, Knut-Frode Dagestad¹, Johannes Röhrs¹, Cecilie Wettre¹, Vassiliki H. Kourafalou², Ioannis Androulidakis², Matthieu Le Hénaff^{3,4}, Heesook Kang², and Oscar Garcia-Pineda⁵

¹Norwegian Meteorological Institute, Allegt. 70, 5007 Bergen, Norway

²University of Miami, Rosenstiel School of Marine and Atmospheric Science, Miami, FL, USA

³University of Miami, Cooperative Institute for Marine and Atmospheric Studies, Miami, FL, USA

⁴NOAA Atlantic Oceanographic and Meteorological Laboratory, Miami, FL, USA

⁵WaterMapping, Gulf Breeze, FL, USA

Correspondence: Lars Robert Hole (lrh@met.no)

Abstract. An open source ocean trajectory framework, OpenDrift, is used to simulate the 2010 DeepWater Horizon oil spill. Metocean forcing data are taken from the GoM-HYCOM 1/50° ocean model with realistic river input and ECMWF global forecast products of wind and wave parameters with 1/8° resolution. OpenDrift includes the integrated oil drift module OpenOil, which includes a number of relevant processes, such as emulsification, wave entrainment, and droplet formation. This takes
5 account of the actual oil type/properties, using the ADIOS oil weathering database of NOAA. The effect of using a newly developed parameterization for oil droplet size distribution is studied, compared to a traditional algorithm. Although the algorithms provide different distributions for a single wave breaking event, it is found that the net difference after long time simulations is negligible, indicating that the outcome is robust regarding the choice of parameterization. In both cases, the size of the droplets controls how much oil is present at the surface and hence are subject to wind and Stokes drift. The oil droplet
10 size is also relevant for the biological impact. Next, the effect of removing river outflow in the ocean model is investigated in order to showcase effects of river induced fronts on oil spreading. A consistent effect on the amount and location of stranded oil is found, and considerable impact of river induced fronts is seen on the location of the surface oil patch. During a case with large river outflow (May 20-27, 2010), the total amount of stranded oil is reduced by about 50% in the simulation with no river input.

15 *Copyright statement.* TEXT

1 Introduction

The presence of both shelf and open sea dynamics makes the Northern Gulf of Mexico (NGoM) a topographically and dynamically complex and interesting study area, in the presence of intense oil exploration. Interactions of the Mississippi River

(MR) plume and the Loop Current (LC) system were found to be important for the transport and fate of oil during the 2010 DeepWater Horizon (DWH) incident (Kourafalou and Androulidakis, 2013; Le Hénaff et al., 2012).

According to the U.S. Energy Information Administration, more than 45% of total U.S. petroleum refining capacity and 51% of total natural gas processing plant capacity is located along the Gulf coast www.eia.gov/special/gulf_of_mexico/. Oil
5 leaks and accidents, such as the explosion on the DWH platform in 2010 (at 28.737°N, 88.366°W), have released significant quantities of hydrocarbons (Crone and Tolstoy (2010); McNutt et al. (2011)) in the sensitive marine environment around the MR Delta, and over the Louisiana TEXas (LATEX) and Mississippi Alabama FLorida (MAFLA) shelves (Kourafalou and Androulidakis, 2013) (Fig. 1).

Many studies have dealt with simulation of the DWH spill (North et al., 2011; Mariano et al., 2011; MacFadyen et al.,
10 2011; Barker, 2011; Le Hénaff et al., 2012; Paris et al., 2012; Kourafalou and Androulidakis, 2013), with focus on both subsurface (Paris et al., 2012) and surface (Le Hénaff et al., 2012) transport. North et al. (2011) used a plume model to predict a stratification-dominated near field, in which small oil droplets detrained from the central plume containing faster rising large oil droplets and gas bubbles and became trapped by density stratification. They showed that simulated droplets with diameters between 10 and 50 μm formed a distinct subsurface plume, which was transported horizontally and remained in the subsurface
15 for >1 month. In contrast, droplets with diameters >90 μm rose rapidly to the surface. Le Hénaff et al. (2012) focused on oil transport on the water surface and found that the wind played a major role in advecting the oil to the northern GOM. Barker (2011) conducted Monte Carlo simulations consisting of 500 individual oil trajectory scenarios using historical data of water currents and winds. The results by Barker (2011) indicated that, in approximately 75% of the scenarios, oil would be transported out of the GOM by the Loop Current. This means that the actual trajectory of oil from the DWH falls in the 25%
20 of scenarios.

Androulidakis et al. (2018b) carried out a field experiment deploying surface drifters at different times near the Taylor Energy Site which is located in the vicinity of the MR outflow region over the NGoM and near the DWH site (approximately at 28.938°N, 88.978°W, Fig. 1). This multi-platform observational experiment was conducted in April 2017 to investigate the main transport pathways from the Taylor Site and toward the NGoM continental shelves and offshore, toward the Gulf interior.
25 Results indicated that the surface transport was determined by the MR plume extension over the Taylor Energy Site and the river induced fronts in combination with local circulation, prevailing winds and broader regional dynamics (LC system). The drifters deployed during the field experiment in tandem with satellite data, drone imagery, wind measurements, and marine radar derived currents and images described three major transport pathways, in agreement with the three major circulation patterns of the MR plume (Schiller and Kourafalou, 2010; Androulidakis et al., 2018a; Schiller et al., 2011; Schiller and
30 Kourafalou, 2014).

The drifters deployed by Androulidakis et al. (2018b) followed the two prevailing coastal currents associated with MR plume dynamics (downstream/upstream moving westward/eastward of the Mississippi Delta) and an offshore pathway under the influence of basin-wide circulation. Near the Taylor site, the existence of multiple river fronts influence the fate of oiled waters, preventing the transport of hydrocarbon toward the delta like a natural boom barrier, trapping and directing the oil
35 either westward or eastward in agreement with Kourafalou and Androulidakis (2013), who showed a similar interaction during

the DWH accident. *In situ* thermohaline measurements around the Taylor Energy Site and across the river front showed that the MR plume near the Taylor Site was 5m to 10m deep, while the clearer ocean water column was characterized by a 40 m upper-ocean homogeneous layer, mainly controlled by temperature.

In this study, an open source Lagrangian oil drift model, OpenOil, has been used to simulate the DWH oil spill evolution. OpenOil takes into account major factors that influence the short term drift of an surface oil slick such as metocean forcing (including Stokes drift), emulsification, evaporation and vertical entrainment and mixing. Dissolution, which is important for subsurface oil spills, is not yet implemented. Simulations are initiated from satellite observations and a point source at the sea floor. The effect of using two different oil droplet size distribution on the horizontal drift and vertical mixing is discussed. Next, the study showcases how NGoM oil pathways are influenced by river plume circulation and river induced fronts. It is also investigated whether the use of realistic daily river discharge has a significant effect on the simulated location of the Surface Oil Patch (SOP) and stranding of oil.

2 Methods and data

2.1 Shapefiles of surface oil patch

Shape files derived from satellite analysis of the DWH SOP can be accessed through the NOAA-ERMA website erma.noaa.gov/gulfofmexico. In the present study, oil particles were seeded uniformly within the region enveloping the thick and thin oil slicks with no distinction. The shapefiles were used here for both initialization of the oil drift simulations and for verification of results.

2.2 Metocean forcing

In the cases presented here, the ocean circulation fields come from a data-assimilative, high-resolution ($1/50^\circ$, 1.8 km) configuration of the Hybrid Coordinate Ocean Model (HYCOM - www.hycom.org) in the Gulf of Mexico (GoM), developed by the authors. This configuration, which we refer to as GoM-HYCOM $1/50^\circ$, uses daily river forcing and data assimilation (GoM-HYCOM $1/50^\circ$). The HYCOM model has a flexible, hybrid vertical coordinate system, in which the distribution of vertical layers is optimized: they are isopycnal in stratified water columns, sigma terrain-following in regions with sharp topography, and isobaric in the mixed layer and very shallow areas (Bleck, 2002). More information about the HYCOM model is available in the model user's manual www.hycom.org and the references therein. The GoM-HYCOM $1/50^\circ$ covers the entire GoM and uses 32 vertical levels. The model configuration is similar to the one used by Le Hénaff and Kourafalou (2016), with the realistic river forcing parameterization developed by Schiller and Kourafalou (2010). The river discharge data were obtained from the Army Corps of Engineers and the U.S. Geological Survey (USGS - www.usgs.gov). The model is initialized in October 2009 with fields from the operational Global HYCOM (GLB-HYCOM) simulation run at the Naval Research Laboratory at the Stennis Space Center (GLB-HYCOM *expt_90.8*, www.hycom.org), and it is nested at the open boundaries with model fields from the same simulation. The atmospheric forcing is based on the 3-hourly winds, thermal forcing and precipitation forecast

fields from the European Centre for Medium-Range Weather Forecasts (ECMWF www.ecmwf.int), with spatial resolution of 0.125° (see below). The model assimilates satellite observations of Sea Surface Temperature and Sea Surface Height, and in situ observations of temperature and salinity from buoys, cruises, surface drifters, Argo floats and XBT casts. More details about the model configuration can be found in Le Hénaff and Kourafalou (2016) and Androulidakis et al. (2018a). For the present study, two simulations were performed: one with the attributes mentioned above, called *Reference* simulation, and one called *No river*, in which the salinity fronts have been removed by shutting off the river discharge, setting precipitation to zero, and turning off the assimilation of salinity profiles. All the other forcing conditions (e.g. meteorological, boundary) remained the same between the two experiments in order to investigate the impact of an individual forcing mechanism (here the Mississippi buoyant discharge and the related density fronts) on the circulation features and furthermore on the oil spill extensions during the DwH period. The outputs from both simulations are available at the Gulf of Mexico Research Initiative Information and Data Cooperative (GRIIDC - data.gulfresearchinitiative.org/).

The ECMWF provides daily global forecasts at 0 and 12 UTC with 0.125° resolution. Recent model upgrades have improved the overall performance of the forecasting system throughout the medium range. Further details on model description and verification can be found e.g. in Ehard et al. (2016), Haiden et al. (2016) and at apps.ecmwf.int/mars-catalogue/?class=od&stream=oper. Here, ECMWF daily forecast products were used as atmospheric upper boundary conditions for the GoM-HYCOM 1/50 as well as for providing air temperature and wind drag for the OpenOil simulations with a 3 hourly time step.

Wave properties were downloaded from the ECMWF third generation spectral Wave Model global operational runs (apps.ecmwf.int/mars-catalogue/?class=od&stream=wave). WAM is well known, see, e.g. Group (1988) and Haiden et al. (2016). The WAM model computes two-dimensional wave distribution, with 25 frequencies and 24 directions. From the two-dimensional spectra, several parameters are computed, including significant wave height, peak wave period, mean wave period, peak wave direction and mean wave direction. The wave parameters are computed for total sea, and for wind sea and swell separately (Haiden et al., 2016). The operational daily WAM forecasts used here are forced by the ECMWF atmospheric forecasts. WAM model output with 0.125° horizontal resolution are downloaded from ECMWF with 12 hourly time step and used here for estimating horizontal Stokes drift and vertical mixing of the oil with a 3 hourly time step using linear interpolation.

Two periods are studied here: 20-27 May 2010 and 2-10 July 2010. According to the ECMWF model, during the first period, wind speed varied between 0.1 and 7.2ms^{-1} and the significant wave height varied between 0.1 and 1.2m . In the second period, the corresponding values were 5 to 12ms^{-1} and 0.1 to 3.2m .

2.3 The oil drift model OpenOil

OpenOil is based on the OpenDrift trajectory modeling framework (Dagestad et al., 2018), developed at the Norwegian Meteorological Institute and available as open source software from www.github.com/opendrft. It is used as the operational oil spill contingency and search and rescue model in Norway. OpenOil has been evaluated against drifter and oil slick observations in the North Sea (Jones et al., 2016; Röhrs et al., 2018). Details of the particle tracking model are given in Dagestad et al. (2018), and model physics that are specific to oil transport and fate are documented in Röhrs et al. (2018) and in the following.

OpenOil is an integrated oil drift model consisting of sub-models for specific physical processes like wave entrainment of oil (Li et al., 2017c), vertical mixing due to oceanic turbulence (Visser, 1997), resurfacing of oil due to buoyancy (Tklich and Chan, 2002), and emulsification taking account for oil properties (Lehr et al., 2002). The resurfacing is a function of oil density and droplet size following Stokes Law, and thereby the model physics are very sensitive to the specification of the oil's droplet size.

Oil droplet size distribution

Several algorithms are implemented to describe the oil's droplet size distribution, based on previous published parameterizations. The first option is based on the work of Delvigne and Sweeney (1988) (DS88), manifesting a power-law droplet size number distribution as a function of droplet size, with an exponent of -2.3, i.e. there are many more small droplets than large droplets. Transferring this to a volume size distribution, as needed for practical oil spill simulation that follows the mass of the oil spill, the exponent becomes 0.7, i.e. there is more volume in the few large droplets than in the many small droplets. The typical droplet sizes range from 1 μm to 1 mm .

A second option to describe the droplet size distribution is based on Li et al. (2017b) (Li17), which takes the oil viscosity and the oil-water interfacial tension into account. This parameterization describes a log-normal law for the number size distribution, and the resulting volume size distribution exhibits a peak at an intermediate droplet size of about 100 μm , depending on oil type and environmental conditions. Similar types of droplet size distribution have been developed and observed, confirming that there is a maximum in oil volume at a particular droplet size (Johansen et al., 2015; Li et al., 2017a).

Following Li et al. (2017b), the volume (V) droplet size spectrum is described by the median droplet diameter, D_{50}^V , as

$$D_{50}^V = d_o r (1 + 10Oh)^p \cdot We^q \quad (1)$$

with the empirical coefficient $r = 1.791$ and the exponents $p = 0.460$ and $q = -0.518$. The PDF for the droplet size distribution follows a log-normal distribution around the medium diameter with a logarithmic base-10 standard deviation of $s = 0.38$ (Eq. 16 in Röhrs et al. (2018)).

The Weber number, We , is a dimensionless number describing the relative importance of inertial forces and oil-water interfacial tension. It is a function of the sea water density, ρ_w , the significant wave height, H_s , and the oil-water interfacial tension, σ_{o-w} , and is given by

$$We = \frac{\rho_w g H_s d_o}{\sigma_{o-w}}, \quad (2)$$

where g is the acceleration of gravity and $d_o = 4\sqrt{\frac{\sigma_{o-w}}{g(\rho_w - \rho_o)}}$ is the Rayleigh-Taylor instability maximum diameter.

The Ohnesorge number, Oh , is a dimensionless number describing the ratio of viscous forces to inertial and surface tension forces. It is a function of the dynamic oil viscosity, μ_o , oil density, ρ_o , and oil-water interfacial tension:

$$Oh = \frac{\mu_o}{\sqrt{(\rho_o \sigma_{o-w} d_o)}}. \quad (3)$$

The volume size distribution, following (Delvigne and Sweeney, 1988), is given by

$$V(d) = d^{-0.6} \text{ for } d_{min} < d < d_{max} \quad (4)$$

where d is the droplet diameter. Minimum and maximum droplet radii are set to $10e-6$ and $10e-3$, respectively. The exponent of -0.7 in the volume size distribution corresponds to an exponent in the number size distribution of 2.3 (Tkalich and Chan, 2002).

Droplet sizes are assigned to oil particles each time a particle is submerged by breaking waves, following the wave entrainment algorithm of (Li et al., 2017c). The implementation of this algorithm in OpenOil is described in full detail in (Röhrs et al., 2018). The droplet sizes for individual particles are drawn from a random distribution according to the chosen size distribution. The size distributions represent conditions for a stochastic wave entrainment event, representing equilibrium conditions during a model time step. It is noted that the overall size distribution of all submerged oil in the simulation is further subject to changes, as weather conditions and the oil's emulsification rate change and oil droplets of various sizes are subject to various resurfacing time scales. Resurfaced particles are considered to be part of a surface slick, and are assigned a new droplet size once they are re-entrained. Oil elements at the sea surface (slick) are not considered to have a radius.

Droplet size distribution during deep blowouts

For oil elements released at the seafloor (wellhead), a simplistic and pragmatic approach of prescribing random radii in the range 0.5 mm to 5 mm was used, as suggested by Johansen (2000).

Horizontal transport

With regard to horizontal drift, three processes are considered: Any element, whether submerged or at the surface, drifts along with the ocean current. Elements are further subject to Stokes drift corresponding to their actual depth. Surface Stokes drift is normally obtained from a wave model, and its decline with depth is calculated as described in Breivik et al. (2016). Oil elements at the ocean surface are additionally moved with a factor of 2% of the wind. Together with the Stokes drift (typically 1.5% of the wind at the surface), this sums up to the commonly found empirical value of 3.5% of the wind speed (Schwartzberg, 1971). The magnitude of the wind drift factor is discussed in Jones et al. (2016) who stated that a 2% wind drift factor was required in OpenOil to reproduce their observations of a SOP in the North sea. In essence, this is believed to be a compensation factor for the inability of any ocean model to represent the strong shear current in the upper few centimeters/decimeters of the ocean, and not surface oil actually moving relative to the water.

The three horizontal drift components may lead to a very strong gradient of drift magnitude and direction in the upper few meters of the ocean. For this reason, it is also of critical importance to have a good description of the vertical oil transport processes.

Vertical transport

Oil elements at the surface, regarded as being in the state of an oil slick, may be entrained into the ocean by breaking waves. The entrainment of oil droplets depends on both the wind and wave (breaking) conditions, but also on the oil properties, such as viscosity, density and oil-water interfacial tension. The buoyancy of droplets is calculated according to empirical relationships and the Stokes law following Tkalich and Chan (2002), dependent on ocean stratification based on temperature and salinity from the ocean model, and the viscosities and densities of oil and water.

In addition to the wave induced entrainment, the oil elements are also subject to vertical turbulence throughout the water column, described using a random-walk scheme based on the turbulent eddy diffusivity from the ocean model.

Weathering

In order to calculate weathering of the oil, OpenOil interfaces with the open source ADIOS oil library, developed by NOAA (github.com/NOAA-ORR-ERD/OilLibrary) and (Lehr et al., 2002). In addition to state-of-the-art parametrization of weathering processes such as evaporation, emulsification and dispersion, this software contains a database of measured properties of almost 1000 oil types from around the world. As oils from different sources or wells have vastly different properties, such a database is of vital importance for accurate results. The ADIOS oil library is also used by the NOAA oil drift model github.com/NOAA-ORR-ERD/PyGnome.

The weathering algorithms describes evaporation and emulsification rate of oil, i.e. the water content. The emulsification and evaporation greatly affect oil density, viscosity and oil-water interfacial tension, and thereby the droplet size distribution through Eqs. 1-3. OpenOil take into consideration weathering processes that are dominating in the initial oil spill period of 2-3 days. Long-term weathering processes such as sedimentation and microbial degradation are not considered in this study.

20 3 Results

A first set of simulations are carried out to investigate the effect of oil droplet size distribution. A second set focuses on the effect of river induced fronts. According to Crone and Tolstoy (2010), the average flow rate from the oil well between 22 April and 3 June 2010 was estimated to $0.1 \text{ m}^3 \text{ sec}^{-1}$, assuming a liquid oil fraction of 0.4. Gas and highly volatile compounds are not considered here. After the riser was removed and until the leak was sealed on 15 July, the flow rate increased to $0.12 \text{ m}^3 \text{ sec}^{-1}$, corresponding to $10,368 \text{ m}^3 \text{ day}^{-1}$. An assumption was made on of how much oil was present at the sea surface at the initialization of the simulation. The residence of oil at the sea surface depends heavily on oil properties as well as environmental conditions such as temperature of ocean and air, wind and waves, as described above. According to our mass balance calculations for the DWH spill, using the Light Louisiana Sweet oil type from the NOAA oil library and environmental conditions as described above, it seems reasonable to assume that 80% of the oil mass is removed from the surface after 10 days. This is within the range in our simulations that is typically 60 to 95% (see examples of mass balance plots further down). While Boufadel et al. (2014) assumed a constant removal rate of surface oil 20% per day, the removal rate in the present

simulation and in reality will vary with wind and wave conditions. The simulations for May 2010 are initialized by seeding 48730 particles in a polygon obtained from NOAA shapefiles. Each particle represents initially 1 m^3 oil. A continuous point source at the sea floor seeds an additional 8460 particles (8460 m^3) per day during the simulation. After June 3rd these numbers are increased by 20% to $10368 \text{ m}^3 \text{ day}^{-1}$. The oil elements released at the surface are assigned droplet radii at each entrainment
5 incident, according to the parameterisation of size distributions from respectively DS88 or Li17, see Röhrs et al. (2018) for details. Oil elements at the sea surface (slick) are not considered to have a radius.

Around 20-25 May 2010 there was a significant outflow of the Mississippi River (Fig. 2) and part of the SOP was entrained along the LC resulting in a formation popularly referred to as the "tiger tail" (Fig. 3). The OpenOil simulation shown on top in Fig. 3 is carried out using the classical DS88 oil droplet size distribution (Delvigne and Sweeney, 1988). Fig. 3 lower panel
10 shows the results from repeating this simulation using the new Li17 formulation. In Fig. 4 the mass balance during seven days for the Li17 simulation is shown. There is virtually no difference between DS88 and Li17 and only Li17 is shown here. Both formulations result in about the same fraction of oil at the surface (about 50%) after 7 days, with moderate wind speeds of up to 7.2 ms^{-1} . The light compounds evaporate fast after release hence the more heavy compounds are tracked here ("dead oil"). Patches of thick oil (where the particles retain nearly 100% of their mass) are visible over a larger area (Fig. 3). Larger oil
15 droplets will rise faster to the surface (North et al., 2011; Röhrs et al., 2018), and DS88 provides a much higher fraction of large droplet after one hour compared to Li17 (Fig. 5, upper panels). However, it turns out that the DS88 and Li17 provide similar volume distributions after a 24 hr test simulation (Fig. 5, lower panels). Still, the peak in the distribution is at around $100 \mu\text{m}$ for both formulations, and rapid rising to the surface can be expected according to North et al. (2011). Due to the small difference between DS88 and Li17, the DS88 simulation results in just marginally more oil stranded after seven days (13.2
20 vs 12.8 %), particularly west of the Mississippi Delta (Figs. 3). A higher fraction of oil at the surface provides more efficient transport by wind and waves towards the shore and larger likelihood of stranding. For both simulations, the oil particles quickly loose 40-50% of their mass, mostly through evaporation.

Fig. 6 shows the geographical distribution of particle diameters at the surface. It is apparent that smaller particles are present outside the MAFLA shelf, probably because the oil particles have been subject to more wind and hence wave action and natural
25 dispersion in the last 24 hours (Fig. 7).

The Li17 formulation is applied for two types of simulations: *Reference* (all forcing data) and *No river* (all forcing data except for river runoff and precipitation). Two periods were chosen for these experiments: a high river discharge period with variable winds (20-27 May) and a relatively lower discharge period with persistent westward winds (2-10 July). The purpose is to investigate the effect of the salinity fronts by using the ocean circulation from the *No river* simulation, in which the
30 precipitation and river discharge are turned off, while atmospheric and wave forcings are kept the same. In Figs. 9, 8, 10 and 11 it appears how the inclusion of river discharge in the ocean forcing can have opposite (and sometimes counter-intuitive) effects on oil transport. Table 1 summarizes the difference of the *Reference* and *No River* simulations for May 20-27, whilst Table 2 shows corresponding values for the 2-10 July simulations.

Kourafalou and Androulidakis (2013), based on high-resolution ocean simulations over the NGoM, showed that the MR
35 discharge peak around 20-30 May led to the formation of downstream (westward) and upstream (northeastward) plume areas

Table 1. Percentages of stranded oil particles for the May 20-27 simulations.

	<i>Reference</i> simulation	<i>No River</i> simulation
West of MR Delta	6.9	0.5
MR Delta area	4.0	3.4
East of MR Delta	1.2	2.1
Total	12.1	6.0

Table 2. Percentages of stranded oil particles for the July 2-10 simulations.

	<i>Reference</i> simulation	<i>No River</i> simulation
West of MR Delta	10.6	7.8
MR Delta area	16.7	27.2
East of MR Delta	20.8	20.1
Total	48.1	55.1

that acted as a conduit for guiding oil toward the LATEX shelf and away from the MAFLA shelf, respectively (Fig. 8). In the 20-27 May period the river plume currents created a strong "bulge" that tended to turn waters clockwise around the Delta, with some waters moving westward. In addition, the offshore GoM circulation (Loop Current and eddies) removed the riverine waters offshore, toward the GoM interior, forming the so-called "tiger tail" pathway. The removal of the MR input in the *No River* experiment during this period (Fig. 9) allowed the spreading of oil toward the western MAFLA shelf due to the absence of this anticyclonic bulge; the stranded oil along the MAFLA coasts is more apparent in the *No River* case in comparison to the *Reference* experiment. In contrast, the amount of stranded oil is less along the western coasts (90W-91W) in the *No River* experiment due to the absence of the downstream MR plume pathway. Moreover, the "tiger tail" signature is weaker in the *No River* simulation. Kourafalou and Androulidakis (2013) showed that the strength of this MR offshore jet could have been an important factor in forming the "tiger tail" oil distribution pattern as also confirmed from satellite and drifter data (Walker et al., 2011).

The second simulation period (2-10 July) was right after another high discharge period (although not as high as in May), promoting again a buoyancy-driven downstream current. This tendency was supported by downwelling-favorable winds (Kourafalou and Androulidakis, 2013), resulting in a clear westward transport of both low-salinity and oil containing waters, along a narrow band (of similar width) close to the LATEX coast and surrounding the Mississippi Delta; extensive coastal areas of stranded oil are apparent along the western coasts in the *Reference* experiment (Figs. 10 and 11). The removal of MR input (*No River* experiment) led to weaker downstream currents both close to the Delta (89.5W) and along the western coasts (west of 90W) and thus less stranded oil over the same region. The anticyclonic bulge, common in strong discharges and source of the downstream current (Kourafalou et al., 1996), is completely absent in the *No River* experiment. As a result, more stranded oil was

computed closer to the Delta, inside Louisiana Bight in the *No River* case. It seems like the absence of the anticyclonic bulge that was able to lead surface oiled waters directly west of the Louisiana Bight allowed the accumulation of oil very close to the Delta. In contrast, smaller differences between the two experiments are detected over the MAFLA region due to the weaker upstream currents during early July (Kourafalou and Androulidakis, 2013). Due to slightly higher wind speed during this period, it appears that most particles have lost 70-90% of their mass due to natural dispersion by waves and evaporation shortly after release (Fig. 10).

4 Discussion and conclusions

Several simulations of the DWH oil spill have been carried out with high resolution forcing data and a Lagrangian oil spill model. Simulations were initialized from satellite observations of the SOP, and a continuous point source with a realistic spill rate at the sea floor.

Our results indicate that the two different formulations for oil droplet size distribution give similar results for both vertical and horizontal distribution of the oil, when wind speeds are typically $5-12 \text{ ms}^{-1}$ and breaking waves can be expected Fig. 3. Both formulations of the oil droplet size distribution result in the characteristic "tiger tail" shape of the SOP for the period 20-27 May 2010, and significant stranding in the delta west of the Mississippi River mouth in line with the observed SOP (see also archive.nytimes.com/www.nytimes.com/interactive/2010/05/01/us/20100501-oil-spill-tracker.html) and (Kourafalou and Androulidakis, 2013).

Both droplet size formulations that are used here (DS88 and Li17) result in similar size distributions after some time of simulation, as seen in Fig. 5. Li17 prescribes a maximum droplet diameter in the volume distribution as seen in Fig. 5, which is due to two regimes in the size distribution where small droplets are limited by viscous effects, and larger droplets by oil-water interfacial tension (Li et al., 2017a). This causes a peak in the volume distribution as seen in laboratory experiments with repeated mixing and wave breaking from the surface. The DS88 distribution does not prescribe such a maximum, using a power-law that increases towards larger droplets in the volume distribution. However, the time-integrated simulations in OpenOil still produce a maximum in the droplet size distribution. The reason for this is the repeated wave breaking at the surface, which is more pertinent to large droplets that quickly rise to the surface. Hence, the description of buoyancy driven resurfacing and wave breaking in the oil spill model, together with the DS88 droplet size spectrum for individual wave breaking events, produces similar results to a more advanced droplet size distribution that explicitly prescribes a maximum in the volume size distribution.

A realistic description of droplet formation is required to describe the effects of an oil spill on the environment (North et al., 2011; Boufadel et al., 2014; Röhrs et al., 2018). Fig. 6 shows that the oil spill transport during the DWH spill favors a transport of small particles towards the northeast, while larger oil droplets follow the paths towards southwest and southeast. As a result of their low buoyancy and turbulent mixing, smaller particles are mixed into deeper parts of the ocean and subject to ocean currents at depth (Röhrs et al., 2018). Larger particles experience stronger buoyancy and are subject to surface currents or return to the surface slick. As wind and waves only affect the near-surface drift, the part of the oil slick that forms large droplets is

quickly separated from the small droplets which retain at larger depths North et al. (2011). This will also impact the effect of the spill on the ecosystem: The parts of the oil spill at the surface is more hazardous to birds and the beach communities, while the small, submerged parts will have a substantially larger surface area to interact with water and plankton (Short, 2017; Carroll et al., 2018).

5 Next, the effect of realistic river discharge on the simulations is studied. One might expect that removing the river discharge would always bring the oil nearer to the shore, but interactions are complex. The *No River* simulation for May 20-27 showed more stranding oil, in particular close to the Louisiana Bight, but less stranding oil further downstream, along the LATEX shelf. The removal of the MR input reduced the downstream currents that were responsible for the westward transport of oiled waters along the LATEX shelf. The MR plume and the accompanying river fronts were responsible to either entrap oil close to the
10 coasts (e.g. LATEX shelf) or keep oiled waters offshore (e.g. MAFLA shelf) due to the the formation of upstream currents (8). These results are in line with (Kourafalou and Androulidakis, 2013) and the NOAA SOP observations used here and shown in 9. It is also obvious that, in the *Reference* simulation, the oil particles are guided by the river fronts and they are carried further away from the coast, pushed into the LC south of 28°N and E of 88.5°W (8).

The second simulation period (2-10 July) was right after a second high discharge period, promoting again a buoyancy-driven
15 downstream current. This tendency is supported by downwelling-favorable winds, resulting in a clear westward transport of both low-salinity and oil-containing waters, along a narrow band close to the LATEX coast and surrounding the Mississippi Delta; extensive coastal areas of stranded oil are apparent along the western coasts in the *Reference* experiment. The removal of MR input (*No river* experiment) led to weaker downstream currents both close to the delta (89.5W) and along the western coasts (west of 90W) and thus less stranded oil over the same region.

20 The simulations presented here were initiated by seeding oil particles evenly in a polygon defined by NOAA satellite products, in addition to a continuous point source at the sea floor. The next possible step is to initiate the simulations from satellite products which contain information about oil film thickness in addition to area, and hence also quantify the amount of oil at the surface.

To the best of our knowledge, this is the first time the importance of the effect of river fronts on oil slick transport in the Gulf
25 of Mexico has been demonstrated using high resolution forcing and a fully fledged oil drift model.

TEXT

Code availability. github.com/OpenDrift/opendrift

Data availability. TEXT

Code and data availability. TEXT

Sample availability. TEXT

Video supplement. TEXT

Appendix A

A1

5 *Author contributions.* TEXT

Competing interests. TEXT

Disclaimer. TEXT

Acknowledgements. This research was made possible by a grant from The Gulf of Mexico Research Initiative (award “Influence of river induced fronts on hydrocarbon transport,” GOMA 23160700). Atmospheric and wave data were kindly provided by the European Center
10 for Medium-Range Weather Forecasts (ECMWF). M. Le Hénaff acknowledges partial support from the Physical Oceanography Division at NOAA’s Atlantic Oceanographic and Meteorological Laboratory, AOML. The outputs from the HYCOM simulations are available at the Gulf of Mexico Research Initiative Information and Data Cooperative (GRIIDC - doi:10.7266/N7NG4NPC).

References

- Androulidakis, I., Kourafalou, V., Le Hénaff, M., Kang, H.-S., and Ntaganou, N.: Loop Current evolution during the Deepwater Horizon oil spill period: the role of mesoscale dynamics over Northwestern Cuba, submitted to *Journal of Marine Systems*, 2018a.
- Androulidakis, Y., Kourafalou, V., Özgökmen, T., Garcia-Pineda, O., Lund, B., Le Hénaff, M., Hu, C., Haus, B. K., Novelli, G., Guigand, C., et al.: Influence of River-Induced Fronts on Hydrocarbon Transport: A Multiplatform Observational Study, *Journal of Geophysical Research: Oceans*, 2018b.
- Barker, C.: A statistical outlook for the Deepwater Horizon oil spill, *Monitoring and Modeling the Deepwater Horizon Oil Spill: A Record-Breaking Enterprise*, 195, 237–244, 2011.
- Bleck, R.: An oceanic general circulation model framed in hybrid isopycnic-Cartesian coordinates, *Ocean modelling*, 4, 55–88, 2002.
- 10 Boufadel, M. C., Abdollahi-Nasab, A., Geng, X., Galt, J., and Torlapati, J.: Simulation of the landfall of the deepwater horizon oil on the shorelines of the Gulf of Mexico, *Environmental science & technology*, 48, 9496–9505, 2014.
- Breivik, Ø., Bidlot, J.-R., and Janssen, P. A.: A Stokes drift approximation based on the Phillips spectrum, *Ocean Modelling*, 100, 49–56, 2016.
- Carroll, J., Vikebø, F., Howell, D., Broch, O. J., Nepstad, R., Augustine, S., Skeie, G. M., Bast, R., and Juselius, J.: Assessing impacts of simulated oil spills on the Northeast Arctic cod fishery, *Marine Pollution Bulletin*, 126, 63–73, 2018.
- 15 Crone, T. J. and Tolstoy, M.: Magnitude of the 2010 Gulf of Mexico oil leak, *Science*, 330, 634–634, 2010.
- Dagestad, K.-F., Röhrs, J., Breivik, Ø., and Ådlandsvik, B.: OpenDrift v1. 0: a generic framework for trajectory modelling, *Geoscientific Model Development*, 11, 1405–1420, 2018.
- Delvigne, G. A. L. and Sweeney, C.: Natural dispersion of oil, *Oil and Chemical Pollution*, 4, 281–310, 1988.
- 20 Ehard, B., Malardel, S., Dörnbrack, A., Kaifler, B., Kaifler, N., and Wedi, N.: Comparing ECMWF high resolution analyses to lidar temperature measurements in the middle atmosphere, *Quarterly Journal of the Royal Meteorological Society*, 2016.
- Group, T. W.: The WAM model—A third generation ocean wave prediction model, *Journal of Physical Oceanography*, 18, 1775–1810, 1988.
- Haiden, T., Janousek, M., Bidlot, J., Ferranti, L., Prates, F., Vitart, F., Bauer, P., and Richardson, D.: Evaluation of ECMWF forecasts, including the 2016 resolution upgrade, *European Centre for Medium Range Weather Forecasts*, 2016.
- 25 Johansen, Ø.: DeepBlow—a Lagrangian plume model for deep water blowouts, *Spill Science & Technology Bulletin*, 6, 103–111, 2000.
- Johansen, Ø., Reed, M., and Bodsberg, N. R.: Natural dispersion revisited, *Marine pollution bulletin*, 93, 20–26, 2015.
- Jones, C. E., Dagestad, K.-F., Breivik, Ø., Holt, B., Röhrs, J., Christensen, K. H., Espeseth, M., Brekke, C., and Skrunes, S.: Measurement and modeling of oil slick transport, *Journal of Geophysical Research: Oceans*, 121, 7759–7775, 2016.
- Kourafalou, V. H. and Androulidakis, Y. S.: Influence of Mississippi River induced circulation on the Deepwater Horizon oil spill transport, *Journal of Geophysical Research: Oceans*, 118, 3823–3842, 2013.
- 30 Kourafalou, V. H., Lee, T. N., Oey, L.-Y., and Wang, J. D.: The fate of river discharge on the continental shelf: 2. Transport of coastal low-salinity waters under realistic wind and tidal forcing, *Journal of Geophysical Research: Oceans*, 101, 3435–3455, 1996.
- Le Hénaff, M. and Kourafalou, V. H.: Mississippi waters reaching South Florida reefs under no flood conditions: synthesis of observing and modeling system findings, *Ocean Dynamics*, 66, 435–459, 2016.
- 35 Le Hénaff, M., Kourafalou, V. H., Paris, C. B., Helgers, J., Aman, Z. M., Hogan, P. J., and Srinivasan, A.: Surface evolution of the Deepwater Horizon oil spill patch: Combined effects of circulation and wind-induced drift, *Environmental Science & Technology*, 46, 7267–7273, 2012.

- Lehr, W., Jones, R., Evans, M., Simecek-Beatty, D., and Overstreet, R.: Revisions of the ADIOS oil spill model, *Environmental Modelling & Software*, 17, 189–197, 2002.
- Li, C., Miller, J., Wang, J., Koley, S. S., and Katz, J.: Size Distribution and Dispersion of Droplets Generated by Impingement of Breaking Waves on Oil Slicks, *Journal of Geophysical Research: Oceans*, 122, 7938–7957, <https://doi.org/10.1002/2017JC013193>, 2017a.
- 5 Li, Z., Spaulding, M., McCay, D. F., Crowley, D., and Payne, J. R.: Development of a unified oil droplet size distribution model with application to surface breaking waves and subsea blowout releases considering dispersant effects, *Marine pollution bulletin*, 114, 247–257, 2017b.
- Li, Z., Spaulding, M. L., and French-McCay, D.: An algorithm for modeling entrainment and naturally and chemically dispersed oil droplet size distribution under surface breaking wave conditions, *Marine pollution bulletin*, 119, 145–152, 2017c.
- 10 MacFadyen, A., Watabayashi, G., Barker, C., and Beegle-Krause, C.: Tactical modeling of surface oil transport during the Deepwater Horizon spill response, *Monitoring and Modeling the Deepwater Horizon Oil Spill: A Record-Breaking Enterprise*, 195, 167–178, 2011.
- Mariano, A. J., Kourafalou, V. H., Srinivasan, A., Kang, H., Halliwell, G., Ryan, E., and Roffer, M.: On the modeling of the 2010 Gulf of Mexico oil spill, *Dynamics of Atmospheres and Oceans*, 52, 322–340, 2011.
- McNutt, M. K., Camilli, R., Guthrie, G. D., Hsieh, P. A., Labson, V. F., Lehr, W. J., Maclay, D., Ratzel, A. C., and Sogge, M. K.: Assessment
15 of flow rate estimates for the Deepwater Horizon/Macondo well oil spill, US Department of the Interior, 2011.
- North, E. W., Adams, E. E., Schlag, Z., Sherwood, C. R., He, R., Hyun, K. H., and Socolofsky, S. A.: Simulating oil droplet dispersal from the Deepwater Horizon spill with a Lagrangian approach, *Geophys. Monogr. Ser.*, 195, 217–226, 2011.
- Paris, C. B., Hénaff, M. L., Aman, Z. M., Subramaniam, A., Helgers, J., Wang, D.-P., Kourafalou, V. H., and Srinivasan, A.: Evolution of
20 the Macondo well blowout: simulating the effects of the circulation and synthetic dispersants on the subsea oil transport, *Environmental science & technology*, 46, 13 293–13 302, 2012.
- Röhrs, J., Dagestad, K.-F., Asbjørnsen, H., Nordam, T., Skancke, J., Jones, C., and Brekke, C.: The effect of vertical mixing on the horizontal drift of oil spills, *Ocean Science Discussions*, 2018.
- Röhrs, J., Dagestad, K.-F., Asbjørnsen, H., Nordam, T., Skancke, J., Jones, C. E., and Brekke, C.: The effect of vertical mixing on the
horizontal drift of oil spills, *Ocean Science Discussions*, pp. 1–32, <https://doi.org/https://doi.org/10.5194/os-2018-100>, <https://www.ocean-sci-discuss.net/os-2018-100/>, 2018.
25
- Schiller, R. and Kourafalou, V.: Loop Current impact on the transport of Mississippi River waters, *Journal of Coastal Research*, 30, 1287–1306, 2014.
- Schiller, R., Kourafalou, V., Hogan, P., and Walker, N.: The dynamics of the Mississippi River plume: Impact of topography, wind and offshore forcing on the fate of plume waters, *Journal of Geophysical Research: Oceans*, 116, 2011.
- 30 Schiller, R. V. and Kourafalou, V. H.: Modeling river plume dynamics with the HYbrid Coordinate Ocean Model, *Ocean Modelling*, 33, 101–117, 2010.
- Schwartzberg, H. G.: The movement of oil spills, in: *International Oil Spill Conference*, 1, pp. 489–494, American Petroleum Institute, 1971.
- Short, J. W.: Advances in understanding the fate and effects of oil from accidental spills in the United States beginning with the Exxon Valdez, *Archives of environmental contamination and toxicology*, 73, 5–11, 2017.
- 35 Tkalich, P. and Chan, E. S.: Vertical mixing of oil droplets by breaking waves, *Marine Pollution Bulletin*, 44, 1219–1229, 2002.
- Visser, A. W.: Using random walk models to simulate the vertical distribution of particles in a turbulent water column, *Mar. Ecol. Prog. Ser.*, 158, 275–281, 1997.

Walker, N. D., Pilley, C. T., Raghunathan, V. V., D'Sa, E. J., Leben, R. R., Hoffmann, N. G., Brickley, P. J., Coholan, P. D., Sharma, N., Graber, H. C., et al.: Impacts of Loop Current frontal cyclonic eddies and wind forcing on the 2010 Gulf of Mexico oil spill, Monitoring and Modeling the Deepwater Horizon Oil Spill: A Record-Breaking Enterprise, *Geophys. Monogr. Ser.*, 195, 103–116, 2011.

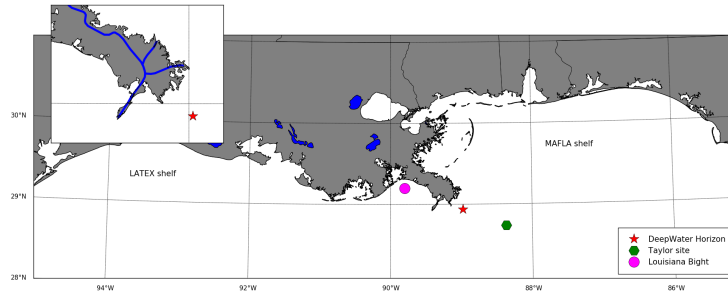


Figure 1. Map of the Northern Gulf of Mexico showing the geographical locations mentioned in the text. The map insert shows the Mississippi River (MR) delta in blue with the three major river passes that release MR water into the Gulf.

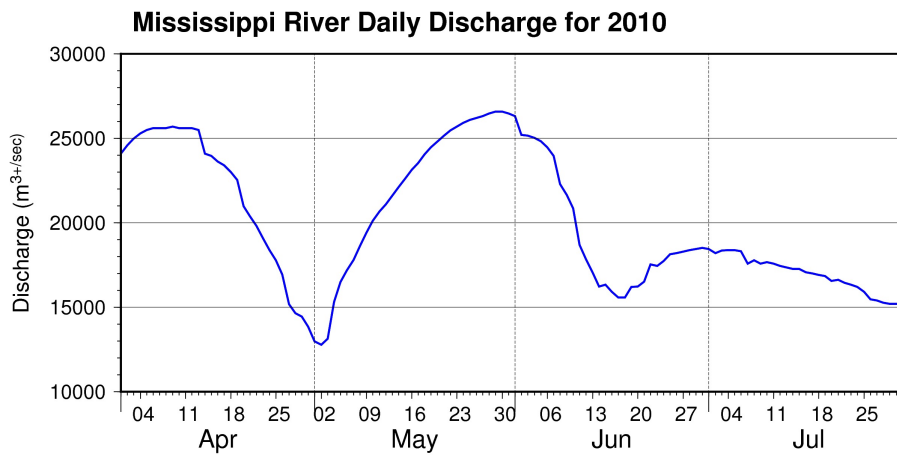


Figure 2. Discharge from Mississippi River in the Northern Gulf of Mexico during late spring and early summer 2010. Data kindly provided by U.S. Geological Survey (USGS www.usgs.gov) and U.S. Army Corps of Engineers

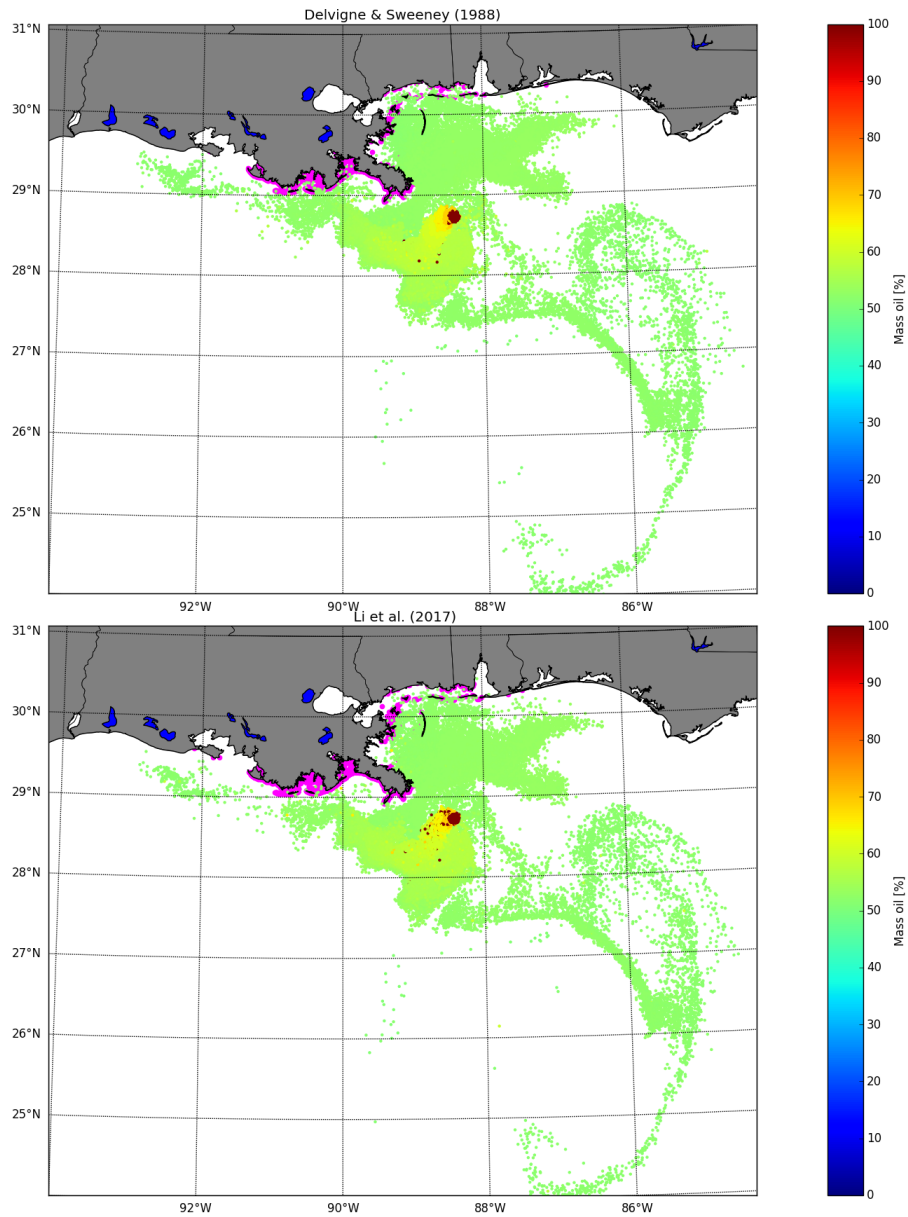


Figure 3. OpenOil simulation for 20-27 May 2010, using the Delvigne and Sweeney (1988) oil droplet size distribution (upper - 13.2% stranded oil), and the Li et al. (2017c) distribution (lower - 12.8% stranded oil). Only surface oil particles are shown. Patch colors are the fraction of mass left in the particles. Magenta areas indicate stranded oil.

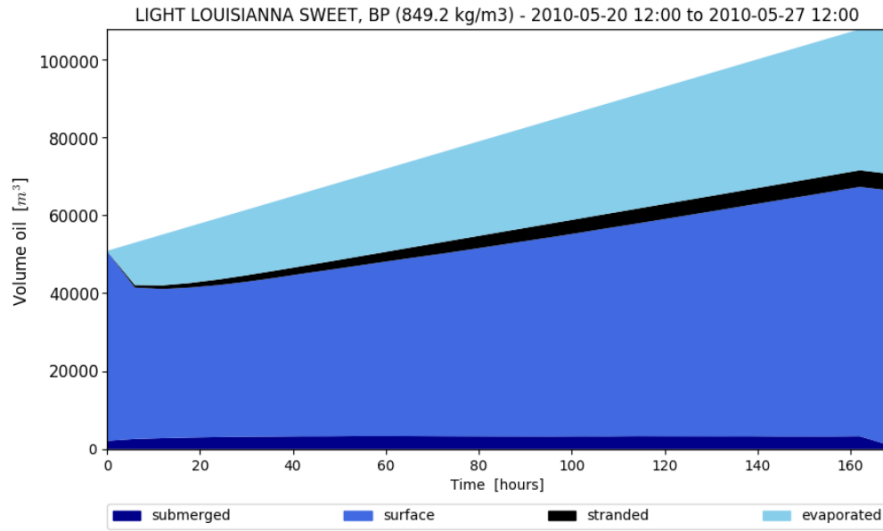


Figure 4. Mass balance of oil in the OpenDrift simulation shown in Fig. 2. The Li et al. (2017c) oil droplet size distribution is used.

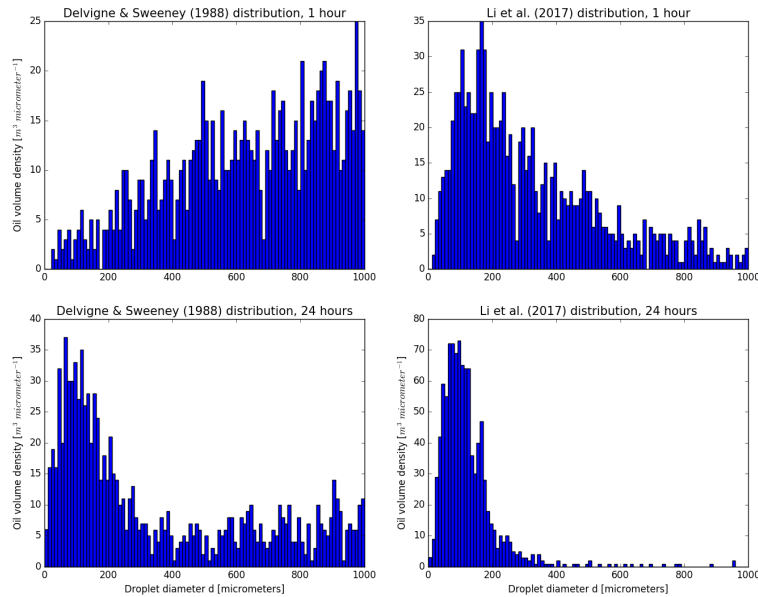


Figure 5. Oil droplet volume histogram for 1000 particles after 1 hours using the *Light Louisiana Sweet, BP* oil type in OpenDrift during 8 ms⁻¹ wind. The initial condition is a uniform distribution. Delvine and Sweeney (1988) formulation at top left and Li et al. (2017c) at top right. Bottom panels show corresponding distributions after 24 hours.

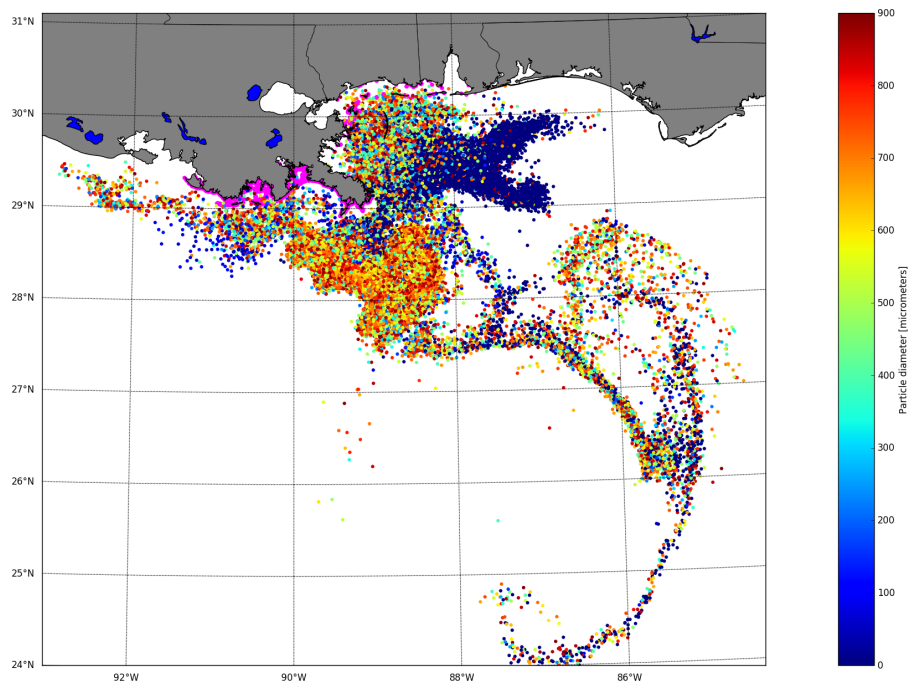


Figure 6. End condition of the *Reference* simulation 20-27 May 2010, showing all active particles (at surface and submerged). Same simulation as in Fig. 3 lower panel. Stranded oil is shown in magenta. The color scale shows diameter of the oil droplets.

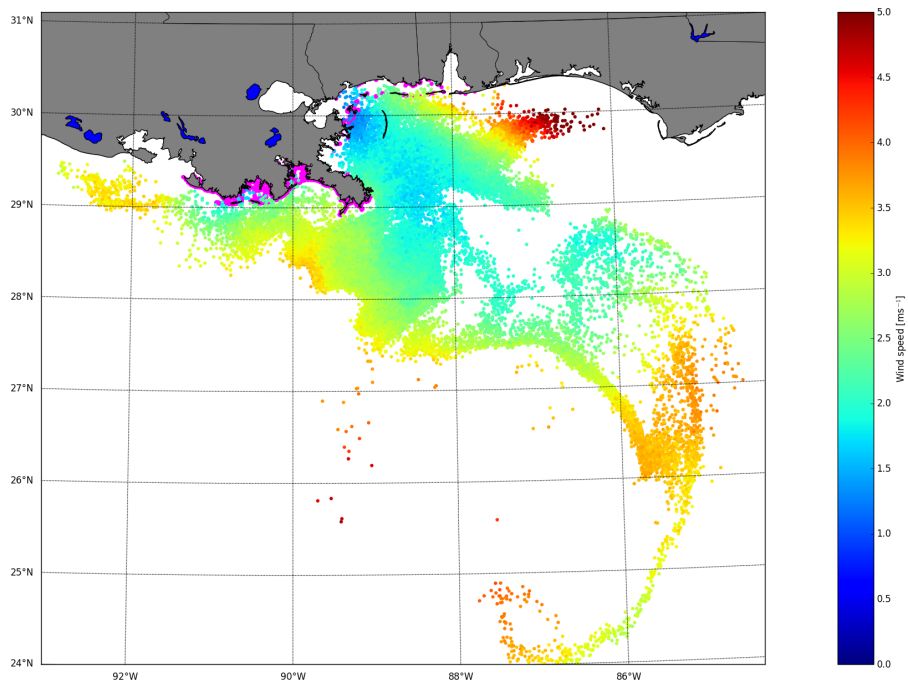


Figure 7. Same as Fig. 6, but the color scale shows the average wind speed experienced by the particle during the last 12 hours.

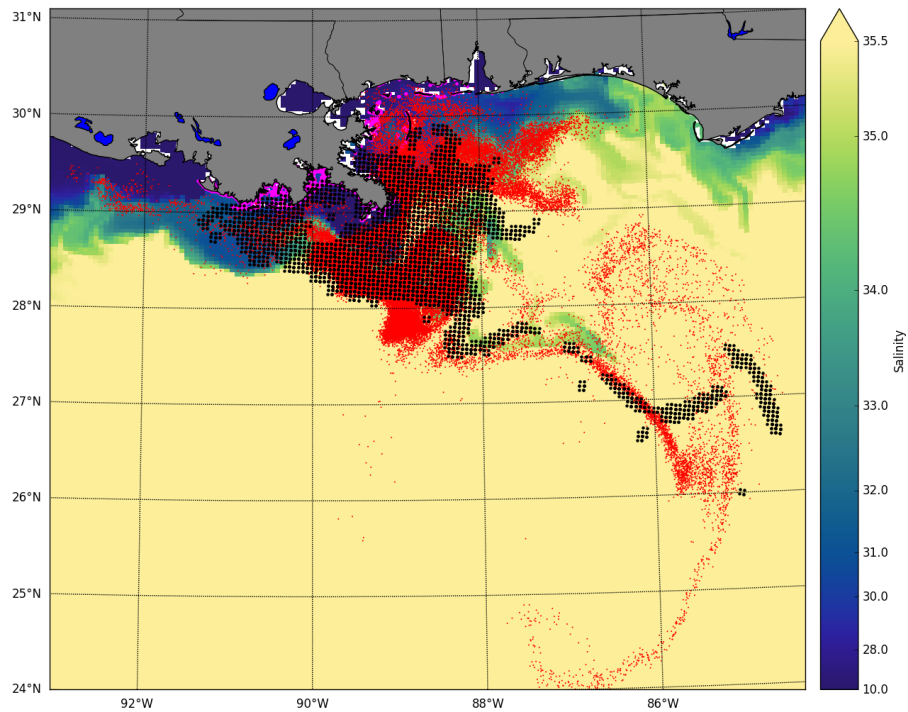


Figure 8. End condition of the *Reference* simulation 20-27 May 2010 (Same simulation as in Fig. 9, upper panel), showing active particles at surface as red dots dots and the corresponding observed surface oil patch (NOAA shape file) as black dots. Modeled stranded oil is shown in magenta. The color scale shows sea surface salinity in the forcing data.

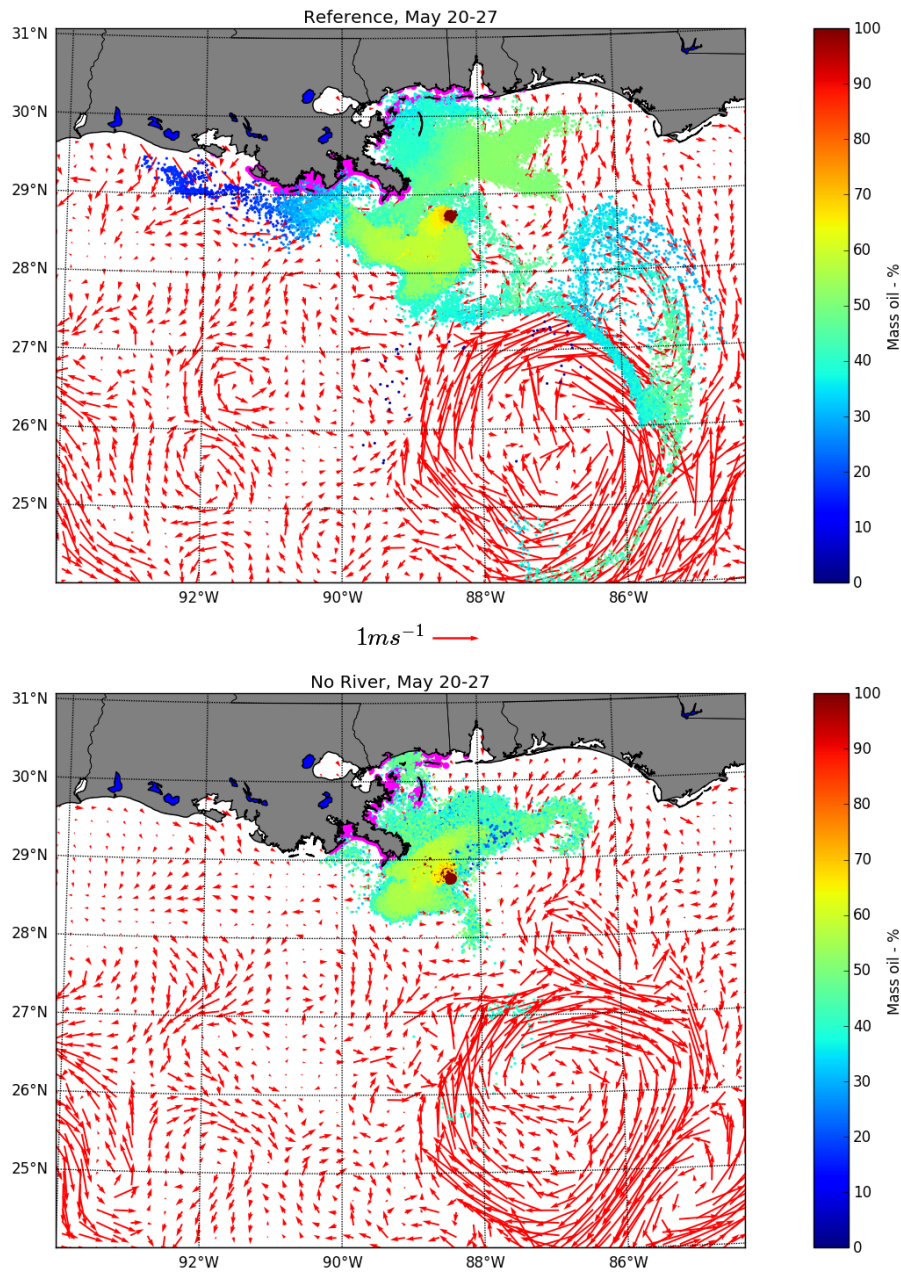


Figure 9. End condition of the simulation 20-27 May 2010, showing active (at surface) and stranded oil particles. Stranded oil is shown in magenta. The color scale indicate how much mass is left in each particle. Red arrows are the GoM-HYCOM 1/50 forcing surface currents at the last time step of the simulation (every 5th data point shown). *Reference* simulation at top (12.1% stranded oil), and *no river* simulation below (5.1 % stranded oil). See also Table 1.

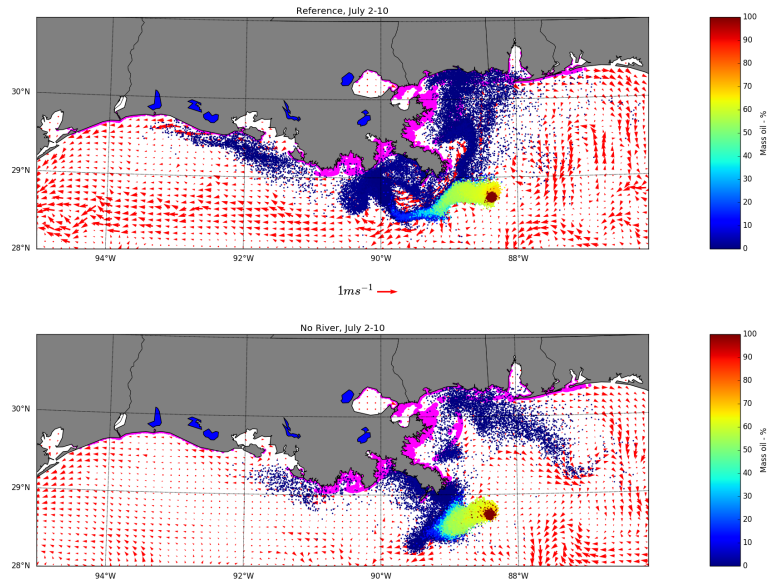


Figure 10. End condition of the simulation 2-10 July 2010, showing active (at surface) and stranded oil particles. Stranded oil is shown in magenta. The color scale indicate how much mass is left in each particle. Red arrows are the GoM-HYCOM 1/50 surface currents at the last time step of the simulation (every 2nd data point shown). *Reference* simulation at top (48.1% stranded oil), and *no river* simulation below (55.1% stranded oil). See also Table 2.

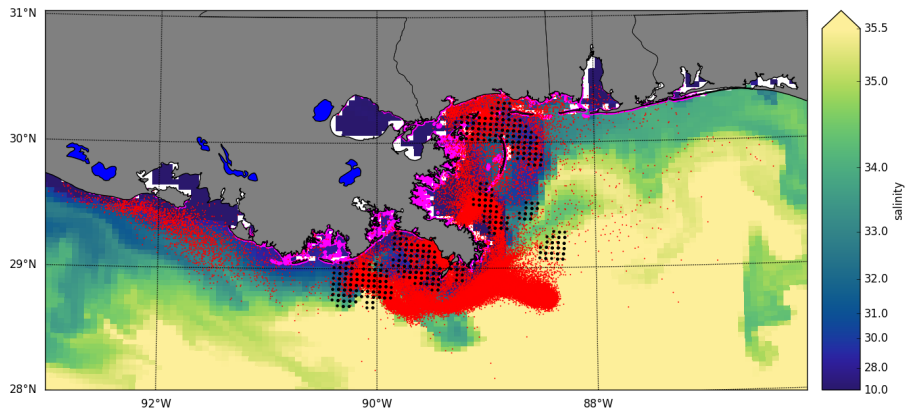


Figure 11. End condition of the *Reference* simulation 2-10 July 2010 (Same simulation as in Fig. 10, upper panel), showing active particles at surface as red dots dots and the corresponding observed surface oil patch (NOAA shape file) as black dots. Stranded oil is shown in magenta. The color scale shows sea surface salinity in the forcing data.